Short Communication

Co and N co-doped porous carbon derived from corn stalk core as electrocatalyst for oxygen reduction reaction in alkaline medium

Liquan Fan[1,], Xinyu Su[1], Tao Cong[1], Yuwei Wang[1], Chaojun Liu[2], Yueping Xiong[2,**]*

[1] College of Materials Science and Engineering, Heilongjiang Provincial Key Laboratory of Polymeric Composite Materials, Qiqihar University, No.42, Wenhua Street, Qiqihar 161006, PR China
[2] School of Chemistry and Chemical Engineering, Harbin Institute of Technology, 92 West Dazhi Street, Harbin 150001, PR China
[*]E-mail: Liquan_Fan@163.com; ypxiong@hit.edu.cn

It is very essential to explore economical non-precious metal catalysts with high performance for the application of a mental-air battery. In this paper, using corn straw core (CSC) as raw material and KOH as activator, the obtained porous activated carbon (AC) with a high specific surface area (1209.1 $m^2 g^{-1}$) and suitable mesopore distribution (~3.8 nm) is prepared through high-temperature carbonization and activation process. The cobalt and nitrogen co-doped activated carbon (Co-N-C) catalyst is obtained by doping cobalt nitrate and urea into AC. The Co-N-C catalyst shows excellent electrocatalytic performance, and the half-wave potential of 0.736 V, the Tafel slope of 108.2 mV dec^{-1}, and the electron-transfer number of around 4 are achieved in 0.1 M KOH. The economic and practical biomass carbon derived from CSC is a kind of promising electrocatalyst for ORR in alkaline medium.

1. INTRODUCTION

The current shortage of resources forces people to start exploring renewable biomass resources. The corn stalk has an ideal sponge-like structure, and the main components are cellulose, hemicellulose, and lignin, which have a large number of pores, thus leading to an ideal specific surface area and mesoporous structure [1-4]. In the process of oxygen reduction reaction (ORR), more active sites would be helpful for the electrocatalytic reaction, to further enhance the reaction activity, which is the major concern for the researchers [5-6], therefore making it urgent and significant to explore novel techniques

or materials for improvement. One of the most common method is doping, which could combine the advantages of both dopant and the main substrate materials. However, the multitype doping based on AC is rarely investigated.

Amongst the metal dopants, platinum is considered to be the most excellent catalyst for ORR [7-8]. However, because of its limited content in nature, non-regenerative characteristic, and high cost, it is necessary to choose other metals to replace platinum [9-13]. Levy and Boudart [14] first discovered the platinum-like properties of transition metal carbides. Since then, non-precious metals, especially transition metals, have been regarded as the best materials to replace platinum catalysts, which has attracted broad attention. For heteroatom doping (N [15], Fe [16,17], Co [18,19], S [20], etc.) into a porous catalyst matrix, there are many factors which affect their performance. First of all, the catalyst matrix needs to have a large specific surface and an appropriate pore size distribution, which can be carried out by adjusting the concentration of activator and activation temperature. It is noteworthy that the electrocatalyst prepared by porous carbon with mesoporous distribution has the most excellent oxygen reduction activity. It is well acknowledged that performance enhancement is usually attributed to pyridinic-N, pyrrolic-N, graphitic-N, and metal-Nx complex [21-23]. Therefore, it is necessary to strictly control the amount of Co and N sources and pyrolysis temperature to fabricate the electrocatalysts with excellent ORR activity. Various kinds of biomass, such as sugarcane [24], sawdust [25], coconut shell [26], rice husk [27], hemp [28], and so on, can be a good candidate for developing porous carbon matrix. Herein, low-cost corn stalks are chosen to be a carbon source as a catalyst matrix, along with cobalt and nitrogen co-doping. The oxygen reduction reaction of the cobalt and nitrogen co-doped activated carbon (Co-N-C) catalyst in alkaline medium is investigated.

2. EXPERIMENTAL SECTION

2.1. Porous carbon preparation

Corn stalks were picked up from local farmland and naturally air-dried for several days to remove moisture. The corn stalks were stripped, sectioned, and chopped into small pieces and dried 60°C for 24 h, followed by being crushed by a grinder and then passed through a 60-mesh sieve to get CSC powder with relatively appropriate particle size. After keeping in Nitrogen gas for half an hour, the CSC was sintered at 400 °C for 2 h at a heating rate of 2.5 °C min^{-1}. The sample after carbonization (CC) was dumped into a 9M KOH solution and stirred for 21 h and sonicated for 3 h. Then obtained powder after filtering was heated at 90 °C for 24 h to remove moisture. Nitrogen was aired for half an hour, and then the sample was sintered from room temperature to 700 °C at 5 °C min^{-1} and kept at 700 °C for 1 h. The obtained powder was dispersed in deionized water and the pH value of the reaction system was adjusted to 7 with 2M HCl. Then the filtered samples were dried in a vacuum drying chamber for a period of 24 h to get black activated carbon (AC), which can be used for preparing the carbon carrier of the catalyst in the next step.

2.2 Catalyst preparation

AC, cobalt nitrate and urea were used as a carrier, cobalt and nitrogen sources, respectively. The three samples, 0.7 g of activated carbon, 0.136 g of urea, and 0.105 g of cobalt nitrate were mixed with 100 mL of ethanol. The mixture solution was stirred for 6 h, and then sonicated for 2 h. Then the filtered powder was placed in a vacuum drying oven to dry at 90 °C for 12 h, and then calcined in a tube furnace in argon and kept at 800 °C for 2h at a heating rate of 2.5 °C min^{-1}. The resultant sample is named Co-N-C. For the sake of comparison, a similar method was used to synthesize cobalt-doped AC (Co-C), using 0.105 g of urea and 0.7 g of activated carbon, and nitrogen-doped AC (N-C), using 0.136 g of urea and 0.7 g of activated carbon as precursors.

2.3 Material Characterizations

The morphology and microstructure of porous carbon and the catalysts were examined by scanning electron microscopy (SEM, Hitachi S-4300) and transmission electron microscopy (TEM, H-7650, Hitachi). The structural information of AC and CC was investigated by X-ray diffraction (XRD, AXS D8, Bruker). The graphitization degree of the sample was analyzed by Raman spectroscopy (labRAM-HR-Evolution, HORIBA). The nitrogen adsorption and desorption tests were carried out using Autosorb-IQ, Kanta Instruments (P/P_0 range from 0.05 to 0.35). The analyses of the specific surface area and pore size distribution were based on Brunauer-Emmett-Teller (BET) and Barrett-Joyner-Halenda (BJH) methods.

2.4 Electrochemical Measurements

The electrochemical measurements were performed at room temperature with an electrochemical workstation (CHI 760E, Shanghai CH Instruments Co., China) and rotating disk electrode (RDE) and rotating ring disk electrode apparatus (RRDE) (RRDE-3A, ALS Co., Ltd., Japan), using a typical three-electrode system. The working electrode of the catalyst-modified glassy carbon electrodes (GCE, 4 mm diameter), the reference electrode of Ag/AgCl, and the counter electrode of Pt wire constitute the three-electrode system. The ORR tests were conducted in 0.1 M KOH electrolyte solution saturated by O$_2$. As for the preparation of the catalyst ink, the procedure was as follows: catalyst powders (3 mg) were dispersed in 1.0 mL of Nafion solution (0.5 wt%), followed by sonication for 30 min to form homogeneous ink. 10mL of the catalyst dispersion inks was deposited onto the surface of GCE. The obtained GCE was dried naturally to serve as the working electrodes. The loading amount of the catalysts was 0.2389 mg cm^{-2}. All of the potentials were converted to refer to the reversible hydrogen electrode (RHE) [29].

3. RESULTS AND DISCUSSION

Fig. 1 illustrates a comparison of XRD spectra of CC, obtained from CSC after carbonization, and AC, obtained from CSC after activation. The diffraction peaks of both CC and AC were broad,

indicating their intrinsic amorphous structure. Their two broad peaks at 23° and 43° correspond to (002) and (100) of amorphous carbon, respectively. The (002) lattice plane is attributed to the interconnection and horizontal stacking of the graphite layer. The (100) lattice indicates that the pyrolytic carbon contains a hexagonal honeycomb structure. Moreover, the diffraction peak of AC is sharper than that of CC, which proves that the AC has a higher degree of graphitization [30-31].
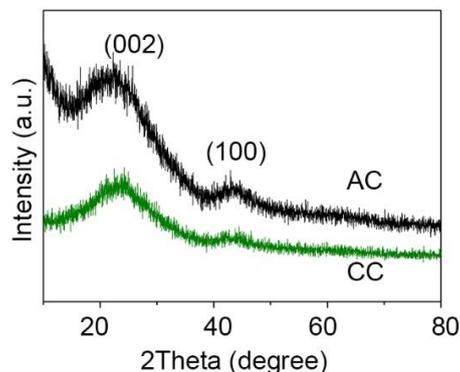
Figure 1. XRD spectra of CC and AC.

Fig. 2a shows the surface morphology of corn stalk core (CSC). The surface of the CSC is very smooth and almost no obvious pores can be observed. Compared with CSC, the surface of the activated carbon (AC) is uneven, and there are many fragments, as shown in Fig. 2b. A typical TEM image, as presented in Fig. 2c, reveals that AC possesses a large number of pores. Due to the result of KOH corrosion, the gas produced in the process of straw and KOH reaction has the effect of opening and expanding holes on straw, thus increasing the number and size of pores. The AC displays the bigger specific surface area relative to the CSC.
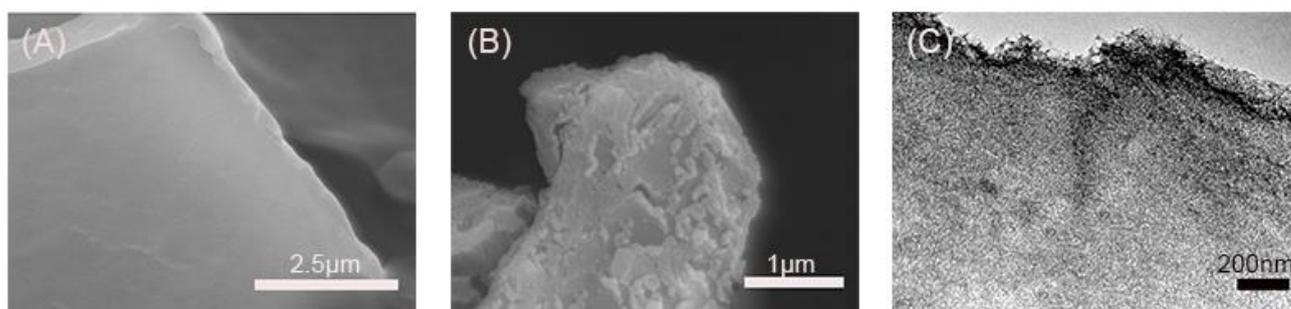
Figure 2. SEM images of CSC (a) and AC (b), TEM image of AC (c)

Brunauer–Emmett–Teller (BET) measurements were conducted to examine the porous nature of the Cobalt–nitrogen-doped AC (Co-N-C). For comparison, the N_2 adsorption/desorption isotherm and the pore-size distributions of AC and Co-N-C are exhibited in Fig. 3. Shown in Fig. 3a, the isotherms are identified as type IV, which is characteristic of mesoporous materials. By contrast, the Co-N-C

possesses a larger number of mesopores than AC. The BET specific surface area of Co-N-C (1403.4 m^2 g^{-1}) obtained by doping is larger than that of AC (1209.1 m^2 g^{-1}). Thus, this implies that the intercalation and migration of metal ions in AC not only increase the defects but also increase the specific surface area, which is beneficial to increase the activity of ORR. The pore sizes calculated using the BJH method were 3.80 nm for AC and 3.82 nm for Co-N-C, respectively, as shown in Fig. 3b. There is little difference in pore size between AC and Co-N-C, and both are standard mesoporous pores. At the same time, it is proved that the AC can be used as a doping matrix.
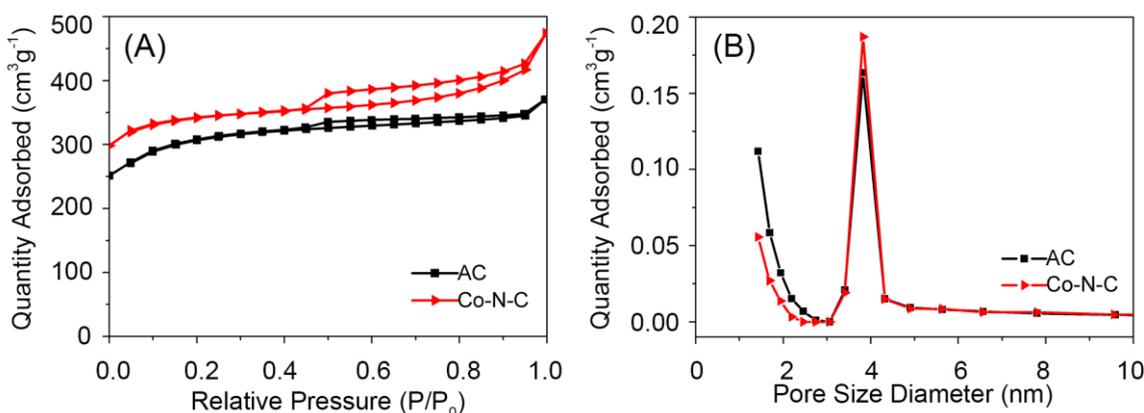
Figure 3. N$_2$ sorption isotherms (a) and pore size distribution plot (b) of AC and Co-N-C.
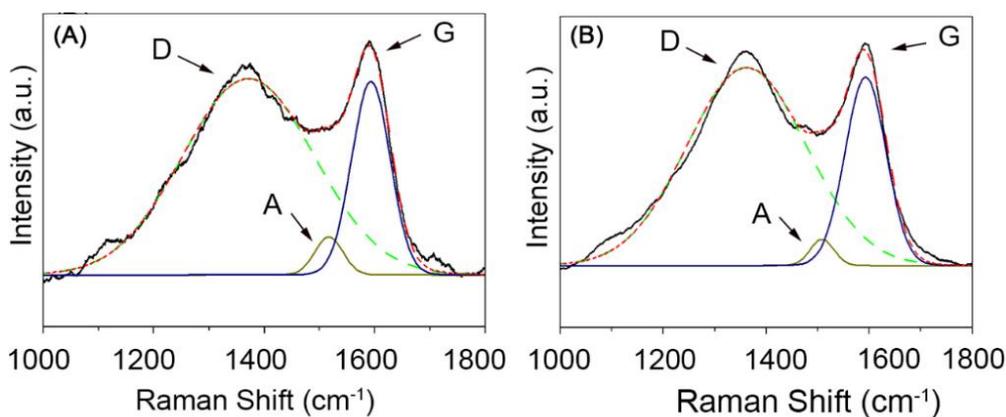
Figure 4. Raman spectra of (a) AC and (b) Co-N-C.
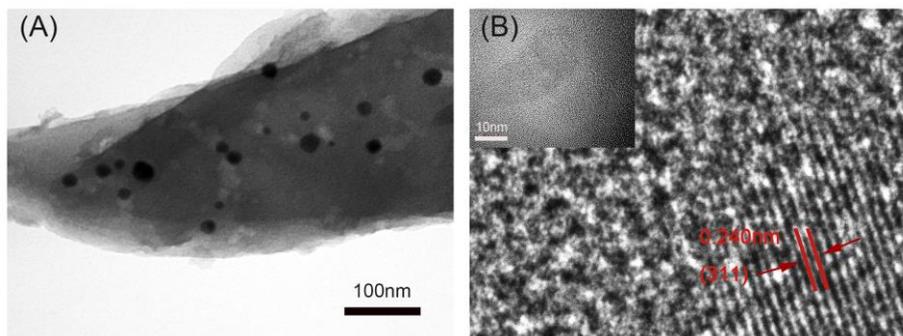
Figure 5. TEM (a) and HRTEM (b) images of Co-N-C

As can be seen from Fig. 4a and 4b, the D band (~ 1340 cm^{-1}) is attributed to the disorder or defects in the lattice of the carbon material. The G peak (~ 1590 cm^{-1}) represents the vibration of sp^2-bonded carbon atoms in 2-dimensional hexagonal lattices. Peak A (~ 1525cm^{-1}) is related to the amorphous carbon structure. The higher the I_D/I_G ratio, the lower the degree of graphitization [32-33]. The peak intensity ratio of Co-N-C ($I_D/I_G = 4$) is greater than that of AC ($I_D/I_G = 3.48$). It can be concluded that the doping of Co and N increased the degree of disorder, which is beneficial to increase the electrochemical performance of the materials.

Transmission electron microscopy (TEM) studies can further reveal that the internal microstructure of Co-N-C, and the black spots in Fig. 5a can be seen that there is Co insertion. Fig. 5b shows a typical high-resolution electron microscopy (HRTEM) image of Co-N-C, and the lattice spacing of 0.24 nm corresponds to the (311) crystal plane of Co_3O_4 and it further confirmed that the Co element has been successfully embedded in the carbon material. The successful insertion of the Co element into Co-N-C can increase the number of electron transfer, make it tend to four electrons, and improve the ORR performance of the catalyst [19].

The electrocatalytic properties of Co-N-C, Co-C, and N-C are compared, as shown in Fig. 6. As shown in Fig. 6a, the polarization curve of ORR shows that the half-wave potential of different samples is different, and the half-wave potential of Co-N-C (0.736 V) is higher than that of Co-C (0.718 V) and N-C (0.657 V). The limit current density of Co-N-C at 0.3 V in Fig. 6b is 5.3 mA cm^{-2}, which is higher than Co-C (4.1 mA cm^{-2}) and N-C (3.6 mA cm^{-2}).
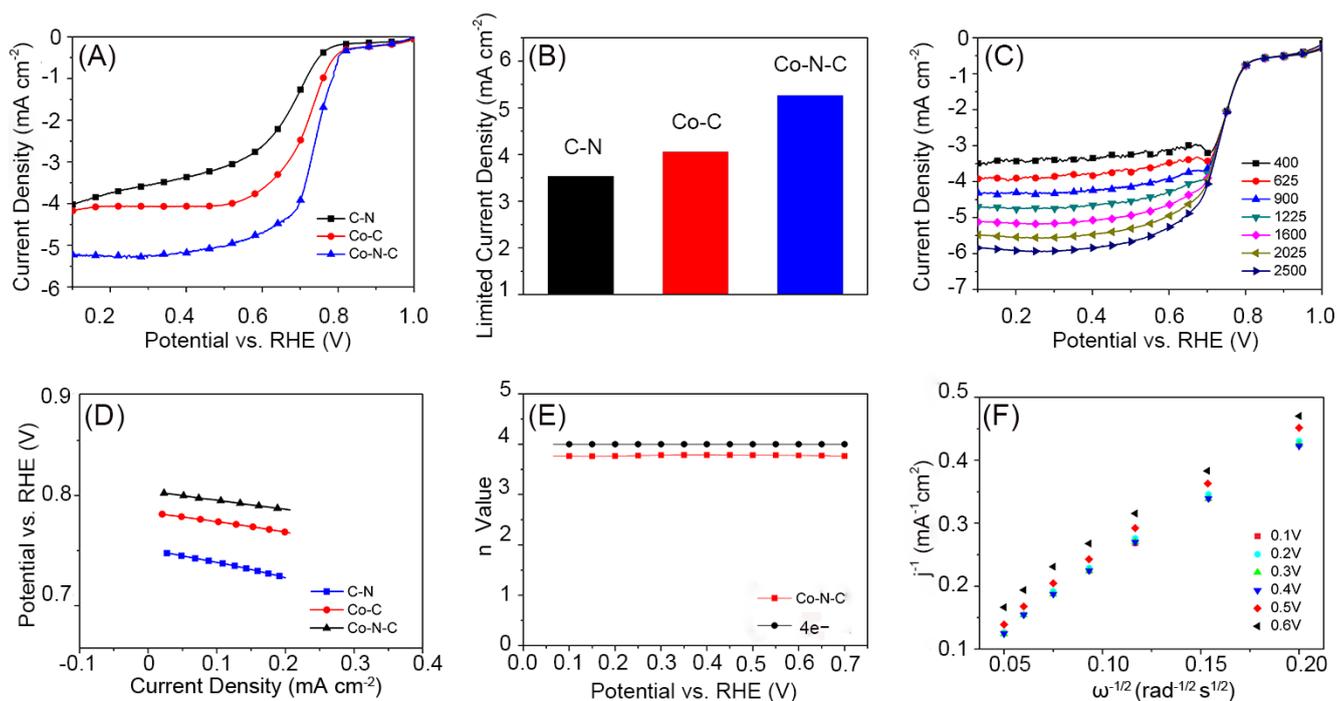
Figure 6. Electrocatalytic performance evaluation of catalysts for ORR in O$_2$-saturated 0.1 M KOH. (a) LSV curves at the rotation rate of 1600 rpm. (b) The limited current densities of the catalysts at 0.3 V. (c) ORR LSV curves at the rotation rates of 400, 625, 900, 1225, 1600, 2025, and 2500 rpm. (d) Tafel plots of different catalysts. (e) The electron-transfer number of Co-N-C (n). (f)The corresponding Koutecky-Levich (K-L) plots of Co-N-C at different potentials.

This is because there are the most active sites in Co-N-C compared with Co-C and N-C. Through the LSV test in O_2-saturated 0.1 M KOH solution at the rotational speed of 400 to 2500 rpm (see Fig. 6c), it is known that the current density increases with the increase of revolutions since the diffusion distance decreases with the increase of rotational speed [34]. Fig. 6d shows Tafel slopes of different catalysts derived from the LSV curves. The performance of Co-N-C (108.2 mV dec^{-1}) is better than that of Co-N (117.9 mV dec^{-1}) and N-C (167.6mVdec^{-1}). It is proved that Co-N-C has excellent ORR dynamics. Fig. 6e shows that the number of transferred electrons (3.78) in Co-N-C approaches 4. It is proved that the main pathway of electron transfer is four electrons. Fig. 6f shows the K-L plots and the calculated electron transfer numbers (n) for Co-N-C is close to 4, which is consistent with the conclusion drawn in Fig. 6e. Based on the abovementioned results, it is proved that Co-N-C has better ORR performance than Co-C and N-C. For the sake of comparison, the electrocatalytic performances of the similar ORR electrocatalysts from the literature [19,35] are summarized in Table 1. As expected, the values in our work are comparable to the best data reported in the literature using the same doping elements composition.

Table 1. Comparison of the electrocatalytic performances with values from the literature for cobalt–nitrogen-doped Carbon.

Sample name	Carbon source	Doping elements	Limited current density at 0.3 V	Half-wave potential	n	References
Co-N-C	cornstalk core	Co, N	5.30 V vs. RHE	0.736 V vs. RHE	3.78	Our work
NCAC-Co	corn stover	Co, N	--	0.743 V vs. RHE	3.87	[19]
NCN-Co-0.1	corn starch	Co, N	--	--	3.90	[35]

4. CONCLUSIONS

Co and N co-doped porous carbon derived from corn stalk core exhibited outstanding ORR performance in 0.1 M KOH medium. Compared with Co-C and C-N, the Co-N-C catalyst showed the highest half-wave potential of 0.736V and the limited current density of 5.3 mA cm^{-2} at 0.3 V and the lowest Tafel slopes of 108.2 mV dec^{-1}. The main pathway of electron transfer for Co-N-C was a 4e$^-$ ORR process with the electron-transfer number of 3.78. CSC after activation was a kind of excellent carbon carrier and after modification of Co and N, it can be used as a promising alternative electrocatalyst in an alkaline medium for ORR reactions. The Co-N-C provides a potential possibility in future application of metal-air batteries.

References

1. K. Yu, H. Zhu, H. Qi, C. Liang, *Diam. Relat. Mater.*, 88 (2018) 18–22.
2. Y.-H. Hwang, S.M. Lee, Y.J. Kim, Y.H. Kahng, K. Lee, *Carbon*, 100 (2016) 7–15.
3. A. Jain, R. Balasubramanian, M.P. Srinivasan, *Chem. Eng. J.*, 283 (2016) 789–805.
4. Q. Wei, X. Yang, G. Zhang, D. Wang, L. Zuin, D. Banham, L. Yang, S. Ye, Y. Wang, M. Mohamedi, S. Sun, *Appl. Catal. B Environ.*, 237 (2018) 85–93.
5. M. Shao, Q. Chang, J.-P. Dodelet, R. Chenitz, *Chem. Rev.*, 116 (2016) 3594–3657.
6. H. Tian, C. Zhang, P. Su, Z. Shen, H. Liu, G. Wang, S. Liu, J. Liu, *J. Energy Chem.*, 40 (2020) 137–143.
7. C. Cui, L. Gan, M. Heggen, S. Rudi, P. Strasser, *Nat. Mater.*, 12 (2013) 765–771.
8. X. Huang, T. Shen, T. Zhang, H. Qiu, X. Gu, Z. Ali, Y. Hou, *Adv. Energy Mater.*, 10 (2020) 1900375.
9. S. Liu, I.S. Amiinu, X. Liu, J. Zhang, M. Bao, T. Meng, S. Mu, *Chem. Eng. J.*, 342 (2018) 163–170.
10. Q. Lv, N. Wang, W. Si, Z. Hou, X. Li, X. Wang, F. Zhao, Z. Yang, Y. Zhang, C. Huang, *Appl. Catal. B Environ.*, 261 (2020) 118234.
11. Z. Pu, C. Zhang, I.S. Amiinu, W. Li, L. Wu, S. Mu, *ACS Appl. Mater. Interfaces*, 9 (2017) 16187–16193.
12. D. Guo, R. Shibuya, C. Akiba, S. Saji, T. Kondo, J. Nakamura, *Science*, 351 (2016) 361–365.
13. Y. Nie, L. Li, Z. Wei, *Chem. Soc. Rev.*, 44 (2015) 2168–2201.
14. R.B. Levy, M. Boudart, *Science*, 181 (1973) 547–549.
15. K. Wan, G.-F. Long, M.-Y. Liu, L. Du, Z.-X. Liang, P. Tsiakaras, *Appl. Catal. B Environ.*, 165 (2015) 566–571.
16. T. Li, M. Li, M. Zhang, X. Li, K. Liu, M. Zhang, X. Liu, D. Sun, L. Xu, Y. Zhang, Y. Tang, *Carbon*, 153 (2019) 364–371.
17. L. Xu, H. Fan, L. Huang, J. Xia, S. Li, M. Li, H. Ding, K. Huang, *Electrochimica Acta*, 239 (2017) 1–9.
18. H.-W. Liang, W. Wei, Z.-S. Wu, X. Feng, K. Müllen, *J. Am. Chem. Soc.*, 135 (2013) 16002–16005.
19. Z. Liu, Z. Li, J. Ma, X. Dong, W. Ku, M. Wang, H. Sun, S. Liang, G. Lu, *Energy*, 162 (2018) 453–459.
20. Q. Wei, G. Zhang, X. Yang, R. Chenitz, D. Banham, L. Yang, S. Ye, S. Knights, S. Sun, *ACS Appl. Mater. Interfaces*, 9 (2017) 36944–36954.
21. H. Liu, M.-Q. Wang, Z.-Y. Chen, H. Chen, M.-W. Xu, S.-J. Bao, *Dalton Trans.*, 46 (2017) 15646–15650.
22. J.C. Carrillo-Rodríguez, I.L. Alonso-Lemus, A.A. Siller-Ceniceros, E. Martínez G, P. Pizá-Ruiz, G. Vargas-Gutiérrez, F.J. Rodríguez-Varela, *Int. J. Hydrog. Energy*, 42 (2017) 30383–30388.
23. B. Bayatsarmadi, Y. Zheng, A. Vasileff, S.-Z. Qiao, *Small*, 13 (2017) 1700191.
24. J. Sreńscek-Nazzal, W. Kamińska, B. Michalkiewicz, Z.C. Koren, *Ind. Crops Prod.*, 47 (2013) 153–159.
25. M. Sevilla, A.B. Fuertes, *Energy Environ. Sci.*, 4 (2011) 1765–1771.
26. J. Chen, J. Yang, G. Hu, X. Hu, Z. Li, S. Shen, M. Radosz, M. Fan, *ACS Sustain. Chem. Eng.*, 4 (2016) 1439–1445.
27. D. Li, T. Ma, R. Zhang, Y. Tian, Y. Qiao, *Fuel*, 139 (2015) 68–70.
28. R. Yang, G. Liu, M. Li, J. Zhang, X. Hao, *Microporous Mesoporous Mater.*, 158 (2012) 108–116.
29. I. Stoševski, J. Krstić, J. Milikić, B. Šljukić, Z. Kačarević-Popović, S. Mentus, Š. Miljanić, *Energy*, 101 (2016) 79–90.
30. Y.J. Hwang, S.K. Jeong, J.S. Shin, K.S. Nahm, A.M. Stephan, *J. Alloys Compd.*, 448 (2008) 141–147.
31. Y.H. Liu, J.S. Xue, T. Zheng, J.R. Dahn, *Carbon*, 34 (1996) 193–200.
32. S.-W. Han, D.-W. Jung, J.-H. Jeong, E.-S. Oh, *Chem. Eng. J.*, 254 (2014) 597–604.
33. J. Liu, Y. Tian, Y. Chen, J. Liang, L. Zhang, H. Fong, *Mater. Chem. Phys.*, 122 (2010) 548–555.

34. Y. Tan, C. Xu, G. Chen, X. Fang, N. Zheng, Q. Xie, *Adv. Funct. Mater.*, 22 (2012) 4584–4591.
35. Q. Zhao, Q. Ma, F. Pan, J. Guo, J. Zhang, *Ionics*, 22 (2016) 2203–2212.